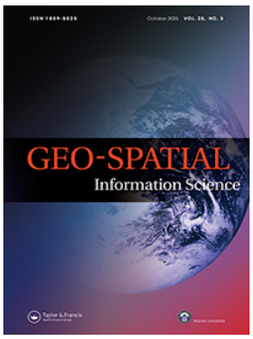

Geo-spatial Information Science

ISSN: 1009-5020 (Print) 1993-5153 (Online) Journal homepage: www.tandfonline.com/journals/tgsi20

Motion-constrained pedestrian tracking framework based on distributed inertial sensors

Lin Qi, Yi Zhang, Yu Liu, Izzy Yi Jian, Yue Yu, Liang Chen & Ruizhi Chen

To cite this article: Lin Qi, Yi Zhang, Yu Liu, Izzy Yi Jian, Yue Yu, Liang Chen & Ruizhi Chen (09 Sep 2025): Motion-constrained pedestrian tracking framework based on distributed inertial sensors, Geo-spatial Information Science, DOI: 10.1080/10095020.2025.2547947

To link to this article: https://doi.org/10.1080/10095020.2025.2547947

Published online: 09 Sep 2025.

GEO-SPATIAL INFORMATION SCIENCE
https://doi.org/10.1080/10095020.2025.2547947

Taylor & Francis
Taylor & Francis Group

Motion-constrained pedestrian tracking framework based on distributed inertial sensors

Lin Qi[a], Yi Zhang[b], Yu Liu[a], Izzy Yi Jian[c], Yue Yu[d], Liang Chen[e] and Ruizhi Chen[e]

[a]Department of Solid-State Image Sensors, The 44th Research Institute of China Electronics Technology Group Corporation, Chongqing, China; [b]Department of Building and Real Estate, The Hong Kong Polytechnic University, Hong Kong, China; [c]Department of Social Sciences and Policy Studies, The Education University of Hong Kong, Hong Kong, China; [d]Department of Land Surveying and Geo-Informatics, The Hong Kong Polytechnic University, Hong Kong, China; [e]State Key Laboratory of Information Engineering in Surveying, Mapping and Remote Sensing, Wuhan University, Wuhan, China

ABSTRACT

The pedestrian tracking and motion detection system (P-TMDS) using distributed inertial sensors has broad application potential toward many emerging fields, such as motion tracking, emergency rescue, and others, due to its advanced autonomous navigation capabilities under signal-denied scenarios. The performance of current P-TMDS is constrained by the cumulative error of low-cost sensors, low accuracy of human motion detection, and lack of effective multi-sensor integration algorithms. This paper proposes a motion-constrained P-TMDS based on the adaptive integration of distributed inertial sensors and ultrasonic ranging (MP-TMDS). An enhanced position–attitude update algorithm is developed for the single-sensor module, which integrates the inertial navigation system (INS) mechanization with multi-level constraints and observations. In addition, a bi-directional long short-term memory (Bi-LSTM) structure is adopted to detect the outlier in ultrasonic ranging results and provide accurate distance observations for dual sensor module-based positioning systems. For the overall MP-TMDS, the measurements provided by distributed sensor modules and ultrasonic ranging are adopted as the input vector of designed spatial–temporal network training for human motion detection and walking speed estimation, and the detected human motion modes are further applied as the constraints for multi-module position–attitude update. Finally, an enhanced data and model dual-driven structure is proposed to adaptively integrate motion features acquired from distributed sensor modules and results of velocity and motion detection provided by spatial–temporal network. Real-world experiments in complex scenes represent that the developed MP-TMDS effectively increases the precision of traditional P-TMDS and outperforms existing algorithms under both positioning and motion detection accuracy indexes, and the estimated accuracy improvement is more than 18.4% compared with state-of-the-art algorithms.

ARTICLE HISTORY
Received 25 July 2024
Accepted 10 August 2025

KEYWORDS
Pedestrian tracking and motion detection; inertial sensors; ultrasonic ranging; deep-learning; data and model dual-driven

1. Introduction

Accurate human tracking and motion detection system (P-TMDS) holds significant potential for applications in numerous emerging fields under urban spaces where the global navigation satellite system (GNSS) is unavailable. Examples of these fields include intelligent elderly care (Qian et al. 2021), emergency response (Zhu et al. 2020), and activity surveillance (Chen, Zhu, and Hammad 2020).

At present, P-TMDS can be realized in two ways: external equipment-supported location systems and independent positioning systems, both of which are widely applied. Especially, for equipment-supported positioning systems, technologies such as Wi-Fi (Yu et al. 2022), Bluetooth (Sun et al. 2021), ultra-wideband (UWB) (Barbieri et al. 2021), sound source (Liu et al. 2024), the 5th generation mobile networks (5G) (Chen et al. 2021a), and micro-electromechanical system (MEMS) sensors (Shi et al. 2022) are commonly used. These technologies provide the public available access to location accuracy from the level of centimeters to room-scale accuracy. However, these positioning systems come with certain constraints. Additional stations are usually required to establish fingerprinting databases or receive wireless observations and are greatly influenced by dynamic and complex urban environments and artificial magnetic interference. Especially under extremely difficult underground or indoor conditions, without enough deployed local stations and supporting facilities, the mentioned approaches cannot achieve efficient and precise indoor positioning. Therefore, they need to be integrated with existing independent location sources to enhance positioning accuracy.

CONTACT Yue Yu michael-yue.yu@polyu.edu.hk

Independent localization systems usually consist of sequence matching that uses acquired magnetic vectors (Kuang et al. 2022), simultaneous localization and mapping (SLAM) (Bao et al. 2022), and multiple source integration (Yu et al. 2023). In this scenario, sequence matching is achieved based on the similarity calculation of magnetic properties between the gathered vector and the reference vector in the database, eliminating the requirement for extra stations. However, at this stage, the frameworks of magnetic matching algorithms necessitate the length of the acquired magnetic sequence and are affected by artificial interference in complex indoor environments (Zhang et al. 2023). In some cases where the magnetic characteristics are not obvious, for instance, long corridors and tunnels, the accuracy of magnetic matching would decrease due to the lack of useful features. Furthermore, visual-based positioning structures are influenced by light change and movement modes, which also leads to the decrease in localization precision (Qin, Li, and Shen 2018). Another effective approach is the distributed built-in sensor positioning systems, by deploying sensor modules into different human body parts, including feet, waist, arms, head, and thigh, to extract comprehensive motion features from the whole pedestrian body and is usually applied in signal-denied areas.

At present, the built-in sensor-based positioning system generally includes two location cumulating approaches: pedestrian dead reckoning (PDR) (Mehrabian and Ravanmehr 2023) and inertial navigation system (INS) (Wu, Kuang, and Niu 2022). The PDR mechanization is made up of four phases: stride recognition, stride-length estimation, heading calculation, and location accumulation. However, a drawback of the PDR mechanization is that the accuracy of the final updated position is influenced by the changeable deployment mode of sensor modules and individual's movement characteristics. Unlike PDR mechanization, INS mechanization is robust to complex motion and handheld modes but is constrained by the fast divergence positioning error.

For applications involving human positioning and motion detection, the distributed built-in sensor-based structure can be classified into a single-module-based approach and multi-module-based approach. Single-module-based approaches typically include foot-mounted positioning systems (FPS) and waist-mounted positioning systems (WPS) that can acquire human motion and location information by only one deployed sensor module. The problem with a single-module-based approach is that the single module cannot effectively represent the full body movement characteristics of a user, and its accuracy is also constrained by cumulative errors, for example, systematic heading error and rough velocity estimation results (Qi et al. 2023). Aiming at the existing challenges of the single-module-based approach, the dual-module-based approach is developed to reduce the systematic heading deviation, and ultrasonic ranging between two feet is also applied to provide more accurate velocity estimation results. Niu et al. (2019) presented that a dual foot-mounted positioning system (D-FPS) does not contain ultrasonic observations to improve the performance of a single-module-based approach, which uses multiple observations and constraints to constrain the effects of systematic heading deviations and inaccurate velocity calculations. Zhu, Wu, and Luo (2021) further integrated the ultrasonic distance measurement results with D-FPS and provided an enhanced multi-source fusion structure to provide accurate walking speed estimation and location update performance.

Furthermore, the combination of FPS modules with WPS modules is able to realize a more comprehensive representation of human motion, and the cooperation of distributed modules can yield more motion-related features and enhance the accuracy of heading and moving velocity calculations. Yu et al. (2019) compared the positioning accuracy and robustness using different modules including FPS, WPS, and smartphones, and various advanced filters were used for multi-source integration. Based on extensive experiments, the waist-mounted method achieves greater precision than the existing methods, and different route paths significantly affect the positioning performance. Qiu et al. (2022) developed a motion tracking system that contains 15 sensor modules to detect the user's motion and position based on the proposed unconstrained traversal algorithm, and gradient descent optimization is used for sensor integration, significantly handling error divergence. The disadvantage of the existing multi-sensor node positioning system is that it cannot effectively mine the constraint relationships between different nodes to cope with complex and disturbed positioning environments, making it difficult to effectively control speed estimation and heading drift errors.

To improve the accuracy of distributed sensor module-based positioning systems, this paper introduces a motion-constrained P-TMDS that merges a wearable sensor network with ultrasonic ranging (MP-TMDS). This system can preserve positioning accuracy in the face of complex pedestrian motion patterns and magnetic disturbances in challenging environments. The innovations of this paper are outlined as follows:

(1) This article extracts multi-level constraints and observations to eradicate the cumulative error caused by low-cost sensor-based INS mechanization. This method independently calculates and compensates for the bias of inertial sensors

using extracted motion features, thereby preserving the accuracy of the single inertial sensor module under long navigation terms.

(2) This article presents a novel dual-module-based position–attitude estimation structure that adaptively merges ultrasonic ranging results and dual-sensor modules. This structure includes a Bi-LSTM-based outlier detector for ultrasonic ranging and an enhanced ellipsoid constraint model for sensor fusion and position–attitude updates.

(3) This article develops a hybrid spatial–temporal network for human walking velocity prediction and motion detection. This method considers and extracts complex motion features provided by distributed sensor modules and ultrasonic ranging and effectively improves the performance of walking speed prediction under different motion modes.

(4) This article introduces a robust data and model dual-driven model (DMDD) that autonomously combines motion data originated from distributed sensor modules and velocity and motion detection results provided by the spatial–temporal model. Multi-level constraints and observations are derived and modeled for improving the accuracy of the whole MP-TMDS structure.

The layout of our paper is organized as follows: Section 2 introduces the single- and dual-module-based positioning algorithms. Section 3 presents the spatial–temporal network-based speed and motion prediction and the overall distributed sensor module-based position–attitude estimation structure. Section 4conducts extensive experiments to validate the presented MP-TMDS.

2. Single- and dual-module-based position–attitude estimator

This part introduces the single-module- and dual sensor-module-based positioning frameworks continuously, in which the single-module positioning system (S-MPS) includes the existing FPS and WPS, while the dual-module-based positioning system (D-MPS) combines two single S-NPSs with ultrasonic ranging modules together for advanced positioning performance. Finally, the overall framework of the proposed MP-TMDS system, which amalgamates three different sensor modules and ultrasonic ranging modules, is described in Figure 1.

2.1. Single-module-based position–attitude estimator

This section proposes a robust single sensor-module-based position–attitude estimator, which can adapt both FPS and WPS by using multi-level constraints and observations to eliminate the cumulative error

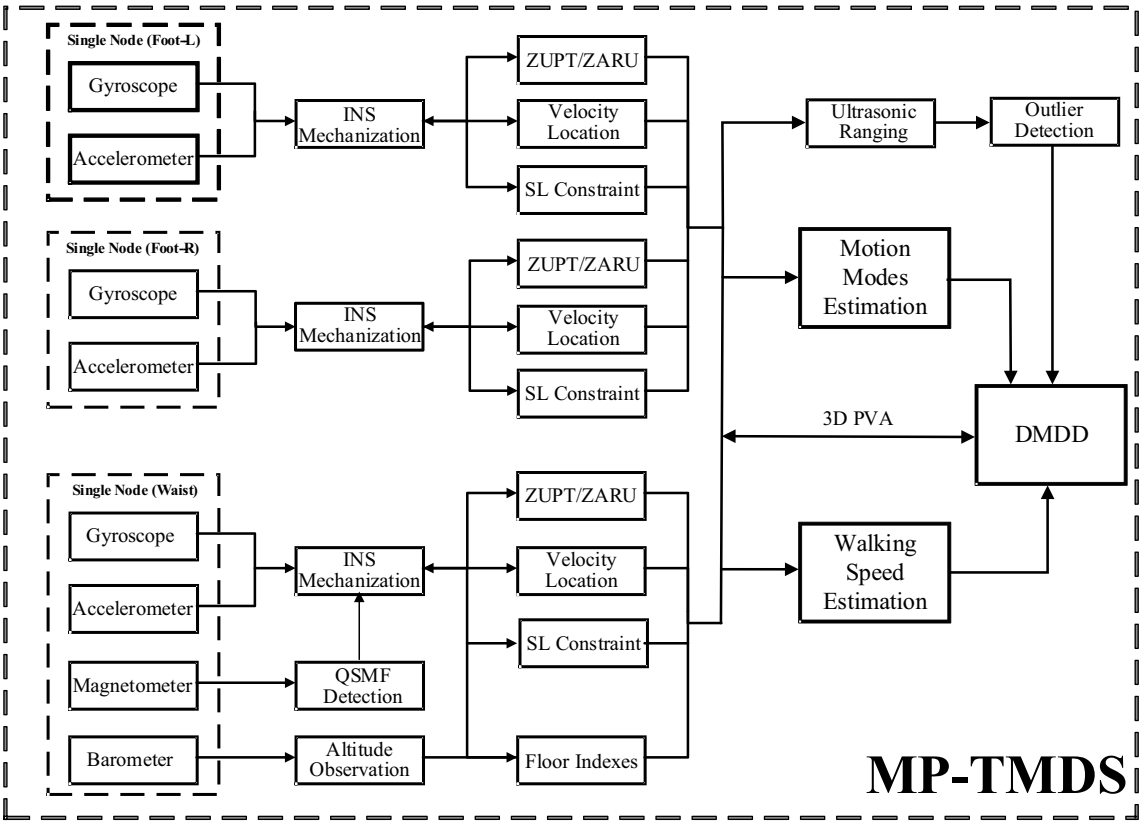

Figure 1. Overall framework of proposed MP-TMDS.

originating from inertial sensors. In the single module-based position–attitude estimator, the INS mechanization is adopted as the basic model for 3D position and attitude update (Qi et al. 2023):

$$\begin{bmatrix} \dot{p}^n \\ \dot{v}^n \\ \dot{C}_b^n \end{bmatrix} = \begin{bmatrix} \varpi^{-1} v^n \\ C_b^n f^b - \left(2\omega_{ie}^n + \omega_{en}^n\right) \times v^n + g^n \\ C_b^n \left(\omega_{ib}^b \times\right) - \left(\omega_{in}^b \times\right) C_b^n \end{bmatrix} \quad (1)$$

where $p^n = [\varphi \quad \lambda \quad h]^T$ indicates the pedestrian's real-time 3D location (latitude, longitude, and height); $v^n = [v_N \quad v_E \quad v_D]^T$ represents the 3D velocity; C_b^n indicates the rotation matrix between body coordinate system and navigation coordinate system; g^n indicates the local gravity value; ω_{ie}^n represents the rotation angular rate between the e-frame and i-frame; ω_{en}^n indicates the rotation angular rate between the navigation coordinate system and the ECEF coordinate system; ϖ^{-1} indicates a 3×3 matrix related to the latitude p_N and the ellipsoidal height h of the moving object.

The Earth rotation-related indicators ω_{ie}^n and ω_{en}^n are able to be omitted due to the high noise level of MEMS sensors, and the simplified state update equation is described as (Niu et al. 2019):

$$\begin{cases} \delta\dot{p}^n = -\omega_{en}^n \times \delta p^n + \delta v^n \\ \delta\dot{v}^n = -\left(2\omega_{ie}^n + \omega_{en}^n\right)\delta v^n + f^n \times \psi + C_b^n(\varepsilon_a + w_{ba}) \\ \dot{\psi} = -\left(\omega_{ie}^n + \omega_{en}^n\right) \times \psi - C_b^n\left(\varepsilon_g + w_{bg}\right) \\ \dot{\varepsilon}_g = \varepsilon_g / \tau_{bg} + w_{bg} \\ \dot{\varepsilon}_a = \varepsilon_a / \tau_{ba} + w_{ba} \end{cases} \quad (2)$$

where $\delta \boldsymbol{p}^n$, $\delta \boldsymbol{v}^n$, and ψ indicate state error values; ε_g and ε_a indicate the biases of gyroscope and accelerometer, respectively; $\boldsymbol{f}^n$ represents the acquired local gravity vector; $\boldsymbol{w}_{bg}$ and $\boldsymbol{w}_{ba}$ represent the noises of sensor measurements.

The state vector of INS mechanization is extracted as:

$$\delta \boldsymbol{X} = [(\delta \boldsymbol{p}^n)_{1\times3} \quad (\delta \boldsymbol{v}^n)_{1\times3} \quad \psi_{1\times3} \quad (\varepsilon_g)_{1\times3} \quad (\varepsilon_a)_{1\times3}] \quad (3)$$

For the foot-mounted positioning system, the quasi-static (QS) periods can be detected and applied for ZUPT update:

$$\delta \boldsymbol{Z}_v^n = \boldsymbol{v}_{INS}^n - \boldsymbol{v}_{zero}^n = \delta \boldsymbol{v}^n + n_v \quad (4)$$

where $\boldsymbol{v}_{INS}^n$ indicates the INS mechanization provided velocity vector; $\boldsymbol{v}_{zero}^n = [0 \quad 0 \quad 0]^T$ indicates the zero-constrained vector. Since ZUPT is unable to constrain the heading drift among QS periods, and ZARU is further proposed for heading alignment (Zhang et al. 2023):

$$\delta \boldsymbol{Z}_\theta = \theta_{INS}^n - \theta_{\text{refer}}^n = \delta\theta + n_\theta \quad (5)$$

where θ_{INS}^n indicates the INS provided heading information, θ_{refer}^n indicates the reference heading observation under the recognized QS phase, and n_θ indicates the Gaussian white noise.

For the low-cost sensor-based INS mechanization, the PDR provided gait-length feature is modeled to constrain the drift error of position–attitude update (Qi et al. 2023):

$$\boldsymbol{V}_{PDR} = \begin{bmatrix} \frac{\alpha_s}{\mu_1 - \mu_0} & 0 & 0 \end{bmatrix} \quad (6)$$

where α_s represents the PDR originated step-length. μ_1 and μ_0 indicate the start and end timestamps of one recognized step period, respectively, and then the PDR updated 2D position is also adopted as one position observation:

$$\begin{bmatrix} r_x^t \\ r_y^t \end{bmatrix} = \begin{bmatrix} r_x^{t-1} \\ r_y^{t-1} \end{bmatrix} + \int_{t-1}^{t} \boldsymbol{V}_{PDR}(k) \begin{bmatrix} \cos(\theta_k) \\ \sin(\theta_k) \end{bmatrix} dk \quad (7)$$

where r_x^t and r_y^t represent the PDR provided 2D position observation; θ_k is the INS mechanization provided heading value.

The overall observation model of PDR mechanization:

$$\begin{cases} \delta Z_v = v_{pdr} - v_{S-NPS} \\ \delta Z_p = P_{pdr} - P_{S-NPS} \end{cases} \quad (8)$$

where v_{pdr} and P_{pdr} represent the 3D location and velocity provided by PDR mechanization, respectively; v_{S-NPS} and P_{S-NPS} indicate the 3D location and velocity provided by INS mechanization, respectively.

To improve the accuracy of positioning, this paper employs the straightline (SL) constraint to minimize the drift error typically observed in conventional walking trajectories (Niu et al. 2021). Additionally, the heading observation derived from successive step intervals is utilized for the identification of SL movement.

$$L_1 = \begin{cases} 1, \max\{|\theta^s - mean(\theta^s)|\} < T_{1,\theta} \\ 0, \text{others} \end{cases} \quad (9)$$

$$\begin{cases} \theta^s = \{\theta_{m-4}^s, \theta_{m-3}^s, \ldots, \theta_m^s\} \\ \theta_m^s = \text{atan2}(r_{y,m}^n - r_{y,m-1}^n, r_{x,m}^n - r_{x,m-1}^n) \end{cases} \quad (10)$$

where $(r_{x,m}^n, r_{y,m}^n)$ indicates the m-th gait location provided by S-MPS; if $L_1 = 1$, the SL constraint can be modeled as:

$$\frac{\theta_m^s - \theta_{m-4}^s}{\Delta t} = [\boldsymbol{0}_{1\times13} \quad \sec\theta \sin\boldsymbol{\phi} \quad \sec\theta \cos\boldsymbol{\phi}]\boldsymbol{X}_t + \varepsilon_\psi \quad (11)$$

where θ and $\boldsymbol{\phi}$ indicate the roll and pitch measurements calculated by S-NPS; ε_ψ indicates the measurement error.

Compared with FPS, the WPS integrates more MEMS sensors, such as magnetometers and barometers, and is necessitated by the inherently rich

features extracted from the motion data they collect, in contrast to the data from foot-mounted positioning systems. As a result, the system leverages the constraint of magnetic vector, stair-originated height, and barometer-derived altitude measurements. The magnetic feature constraint is specifically articulated in Equation (34) within the final MP-TMDS.

In complex 3D environments that encompass multiple levels, the estimation of altitude is of paramount importance, particularly when tracking pedestrian movement on staircases. This study adopts stair-extracted altitude observations, which are carefully modeled to decrease the altitude update error inherent in S-MPS:

$$\delta Z_h = h_{stair} - h_{S-MPS} \tag{12}$$

where h_{stair} is the altitude observation originating from stair observations; h_{S-MPS} indicates the S-MPS originating height information.

Although the accuracy of attitude determination via the S-MPS is prone to rapid error accumulation, the waist-mounted positioning system mitigates this issue by incorporating an altitude constraint derived from barometric readings for effective divergence error control (Shi et al. 2022):

$$\delta z_h^n = h_B^n - h_{INS}^n \tag{13}$$

where h_B^n is the barometer-originated altitude information, h_{INS}^n is the height information provided by S-MPS

2.2. Dual-module-based position–attitude estimator

As elucidated in the previous section, the S-MPS typically integrates the INS mechanization and the QS detection results and employs multi-tiered constraints for ZUPT/ZARU and the SL observation. Nevertheless, the challenge of effectively mitigating the inherent systematic heading deviation associated with the S-MPS necessitates the development of the D-MPS. This system is specifically engineered to minimize the systematic deviation when deploying S-MPS. The presented D-NPS encompasses three distinct multi-source fusion structures of the S-MPS. The fundamental state vector of the D-MPS is constructed using a dual-subsystem approach, which encompasses different FPSs:

$$X^{All} = \begin{bmatrix} X^{(01)} & X^{(02)} \end{bmatrix} \tag{14}$$

where $X^{(01)}$ and $X^{(02)}$ indicate state vectors of single foot-mounted S-MPS, and the state update equation is described as:

$$\delta X_i^{All} = F_{i-1}\delta X_{i-1}^{All} + G_{i-1}w_{i-1}^{All} \tag{15}$$

where w_{i-1}^{All} indicates noise vectors which follow the Gaussian distribution; F_{i-1} indicates the augmented state matrix, and G_{i-1} indicates the augmented noise gain matrix.

In this paper, the Bi-directional Long Short-Term Memory (Bi-LSTM) structure (Pham and Suh 2021) is utilized for outlier detection of ultrasonic ranging results between two feet. The input vector of the Bi-LSTM network is extracted based on the combined motion and ranging information provided by sensors and ultrasonic modules, and the input features of Bi-LSTM are extracted as:

(1) Quasi-static (QS) indexes κ_i of dual foot-mounted modules provided by 1D-CNN.
(2) Distance measurement results D_i^S calculated by the dual foot-mounted modules.
(3) Distance measurement difference ΔD_i^S calculated by the dual foot-mounted modules.
(4) Distance measurement results D_i^U calculated by the dual foot-mounted modules.
(5) Distance measurement difference ΔD_i^U provided by the ultrasonic module.
(6) Residual $\varpi = \left| D_i^S - D_i^U \right|$ between ultrasonic and sensor modules based ranging results.
(7) Walking speed V_i estimated by the waist-mounted module.

Subsequently, the output features of the presented Bi-LSTM are utilized as the input features for the MLP network, and the reference ultrasonic outlier detection result is designated as the output vector:

$$\psi_t = MLP(h_t) \tag{16}$$

where ψ_t represents the ultrasonic outlier detection result with the classification of 0 and 1.

Subsequently, the ultrasonic distance measurement results are utilized as one of the multi-level constraints in conjunction with the positions of FPS modules to reduce the systematic heading deviation. Initially, for the D-MPS, the observation model is formulated as follows (Qi et al. 2022):

$$\delta Z = D_{FPS} - D_{ultra} \tag{17}$$

where $\boldsymbol{Z}$ denotes the discrepancy between the distance measured by ultrasonic signals and the S-MPS for the different feet. An analysis of the D-MPS step dynamics reveals that the inter-foot distance is a variable and can be defined as follows:

$$D_{FPS} = HX_i + \omega_i \tag{18}$$

$$H = \begin{bmatrix} I_3 & 0_{3,12} & -I_3 & 0_{3,12} \end{bmatrix} \tag{19}$$

In the multi-source fusion step, the ultrasonic outlier detector is employed to recognize and eliminate captured abnormal values to enhance the raw

measurements. This procedure aids in maintaining the positioning accuracy of D-MPS.

3. Motion-constrained pedestrian tracking system

In this section, the subsystems of WPS and FPS modules are combined for more accurate recognition of pedestrian motion modes and positions. A hybrid deep-learning model is suggested for simultaneous walking speed estimation and human motion detection, utilizing the information provided by sensor nodes and ultrasonic modules. Furthermore, a data and model dual-driven structure is developed for adaptive integration of distributed modules. The structure of the MP-TMDS is illustrated in Figure 2:

3.1. Hybrid human motion and walking speed estimator

The efficacy of S-MPS is subjected to the intricacies of user motion and the accumulation of errors. To address these challenges, this part introduces a novel spatial–temporal-based estimator for motion and walking speed. The designed spatial–temporal model comprehensively combines LSTM and GCN networks and considers both spatial and temporal features extracted from the sensor-originated motion data. This estimator synergizes features extracted from various nodes to accurately determine human motion modes and provide a reliable reference for walking speed. Unlike the instantaneous models explored in prior research, this part develops a hybrid deep-learning framework for walking speed estimation. This framework considers motion features derived from a period of motion and ultrasonic ranging data outputs from distributed sensor modules. The architecture of the designed spatial–temporal network is illustrated in Figure 3.

Figure 3 presents the basic model of the proposed spatial–temporal network. For the temporal part, we mainly use the LSTM backbone for feature extraction. Specifically, we define the state at each time point as $\boldsymbol{X} \in \mathbb{R}^{f \times t}$, where f is the dimension of features, and t is the number of time steps. The LSTM contains a cell state C_t and a hidden state H_t. At each round t, the

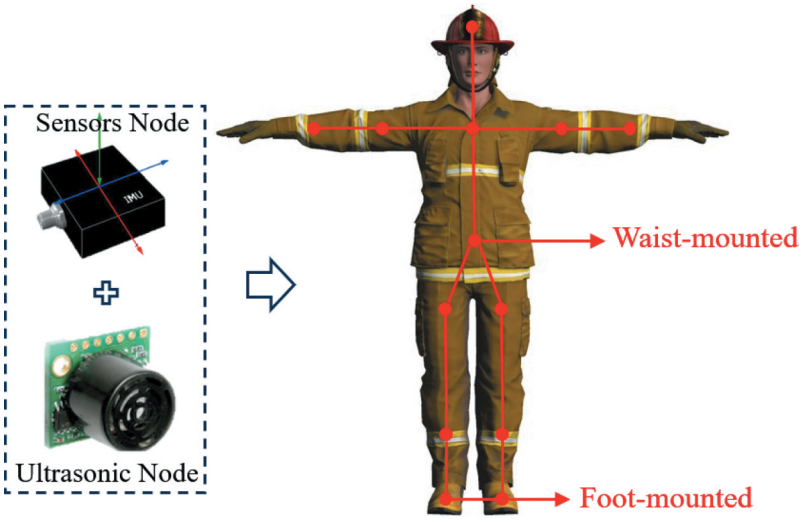

Figure 2. Hardware deployment of proposed MP-TMDS.

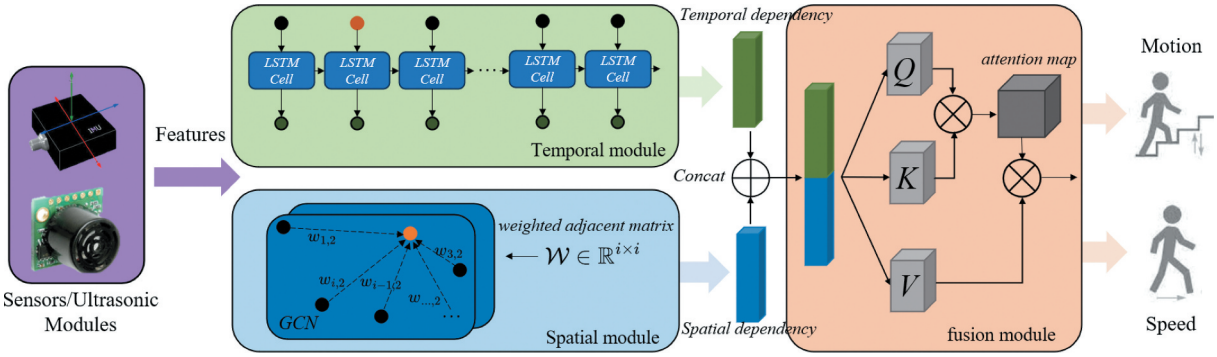

Figure 3. Structure of the spatial–temporal model.

LSTM takes input x_t and previous hidden state H_{t-1} and then updates the states as:

$$\begin{cases} i_t = \sigma(W_{xi}x_t + W_{hi}H_{t-1} + W_{ci}C_{t-1} + b_i) \\ f_t = \sigma(W_{xf}x_t + W_{hf}H_{t-1} + W_{cf}C_{t-1} + b_f) \\ C_t = f_t \,\mathrm{e}\, C_{t-1} + i_t \,\mathrm{e}\, \tanh(W_{xc}x_t + W_{hc}H_{t-1} + b_c) \\ o_t = \sigma(W_{xo}x_t + W_{ho}H_{t-1} + W_{co}C_t + b_o) \\ H_t = o_t \,\mathrm{e}\, \tanh(C_t) \end{cases} \tag{20}$$

where σ is the sigmoid function, and e denotes element-wise multiplication. The LSTM can capture long-term dependencies and model the temporal dynamics in the sequence.

For the spatial part, we mainly use the graph neural network to extract features. Specifically, we define the spatial information as a graph $\boldsymbol{G} = (\boldsymbol{V}, \boldsymbol{A})$, where $\boldsymbol{V}$ is the feature of nodes, i.e. the positions, and $\boldsymbol{A} \in \mathbb{R}^{n\times n}$ is the set of edges for describing the relationship between the positions at each time step. However, in real situations, it is difficult to describe the relationship between various locations by a fixed matrix, so here, we use a matrix $\boldsymbol{A}$ that can be learned to describe the spatial relationships at different timestamps. The graph convolutional network (GCN) is a state-of-the-art (SOTA) graph neural network that can extract features from graph-structured data. The output $\boldsymbol{H}^{l+1} \in \mathbb{R}^{n\times f}$ of the l^{th} layer of GCN is computed as:

$$\boldsymbol{H}^{l+1} = \sigma(\hat{\boldsymbol{A}}\boldsymbol{V}^l\boldsymbol{W}^l) \tag{21}$$

where $\hat{\boldsymbol{A}} = \boldsymbol{D}^{-1/2}\boldsymbol{A}\boldsymbol{D}^{-1/2}, \boldsymbol{A} = \boldsymbol{A} + \boldsymbol{I}_n, \boldsymbol{D}_{ii} = \sum_j \boldsymbol{A}_{ij}$, $\boldsymbol{W}^l$ is the weight matrix, and σ is the activation function. By stacking multiple graph convolution layers, the network can aggregate spatial features from a node's wider neighborhood. The graph structure provides an explicit model for capturing interactions between spatial entities.

After extracting the spatial and temporal features, we use the fusion module to fuse these features. Specifically, we employ the attention mechanism to fuse the features in a learnable way. The attention mechanism is a popular method for learning the relationship between different features. Denote the combined features as $\boldsymbol{X}_c \in \mathbb{R}^{n\times(d_1+d_2)}$, where N is the number of spatial units, and d_1 and d_2 are the feature dimensions of the outputs. The self-attention mechanism learns a soft alignment between each pair of spatial and temporal features, capturing the relevance between them. Formally, the output of self-attention mechanism $\boldsymbol{Z}$ is computed as:

$$\boldsymbol{Z} = soft\max(\frac{\boldsymbol{Q}\boldsymbol{K}^T}{\sqrt{d_k}})\boldsymbol{V} \tag{22}$$

where $\boldsymbol{Q} = \boldsymbol{X}_c\boldsymbol{W}^Q$, $\boldsymbol{K} = \boldsymbol{X}_c\boldsymbol{W}^K$, $\boldsymbol{V} = \boldsymbol{X}_c\boldsymbol{W}^V$, with $\boldsymbol{W}^Q$, $\boldsymbol{W}^K$, and $\boldsymbol{W}^V$ being the learnable parameters of the query, key, and value, and d_k is the dimension of the key vectors.

To achieve better performance of simultaneous human motion detection and walking speed prediction, the following features are calculated based on the extracted motion features of sensors and ultrasonic modules, in which the following motion modes are considered during the model training, prediction, and multi-source fusion phases: static, typical walking, running, backward walking, lateral walking, go up/downstairs, and taking elevator. The input values for the proposed spatial–temporal network are shown as:

1) Collected 3-axis acceleration data a_x, a_y, a_z, and related norms of acquired acceleration vectors extracted from all the foot-mounted and waist-mounted modules:

$$Norm_{acc} = \sqrt{{a_x}^2 + {a_y}^2 + {a_z}^2} \tag{23}$$

2) Collected 3-axis angular rate data g_x, g_y, g_z, and related norms of acquired gyroscope data extracted from all the foot-mounted and waist-mounted modules:

$$Norm_{gyro} = \sqrt{{g_x}^2 + {g_y}^2 + {g_z}^2} \tag{24}$$

(1) Variances of calculated norms of acceleration and angular rate vectors σ_g^2 and σ_a^2.
(2) The barometer-originated altitude change value Δh_B^n provided by waist-mounted module (Qi et al. 2022).
(3) Foot-mounted modules provided velocity values v_1 and v_2.
(4) Distance measurement result u_1 originated from ultrasonic ranging.
(5) Distance measurement difference u_2 originated from ultrasonic ranging.
(6) Walking velocity value provided by the WPS module using the linear step-length equation:

$$L_1 = \frac{\alpha \cdot [0.7 + \beta(H - 1.75) + \varsigma \cdot \frac{(F_t - 1.79)H}{1.75}]}{t_1 - t_0} \tag{25}$$

in which α, β, ς are the human body characteristics, F_t is the gait frequency, and H is the height information.

9) Walking velocity values provided by the WPS module using the nonlinear step-length equation:

$$L = K\sqrt[4]{A_{\max} - A_{\min}} \tag{26}$$

where $A_{\max}$ and $A_{\min}$ indicate the detected peak and valley values of accelerometer data in one gait phase, and K is the scale parameters.

10) Updated frequency F_t of gait-length provided by the WPS module.

The output dimension of the developed motion and walking speed estimator contains 1D walking speed prediction results and types of human motion modes described by the number indexes from 0 to 7, considering the impact of complex pedestrian motion modes

on the walking speed estimation. Hence, the presented spatial–temporal network efficiently integrates the influence of complex human motio, and feedback motion features into the estimated human velocity, which is further applied as a constraint vector in the final DMDD structure.

3.2. Data and model dual-driven based fusion structurer

This section proposes a novel DMDD structure, taking into account the human motion features extracted from hybrid sensor modules, the ultrasonic ranging module, magnetic reference, and the output of the spatial–temporal model. This structure achieves an adaptive combination of indoor positioning using distributed MEMS sensor modules. The overall state vector of the proposed MP-TMDS, which includes three different sensor node-based subsystems, is modeled as follows (Zhu, Wu, and Luo 2021):

$$X^{All} = \begin{bmatrix} X^1_{sub} & X^2_{sub} & X^3_{sub} \end{bmatrix} \tag{27}$$

where X^1_{sub} and X^2_{sub} are state vectors of foot-mounted modules; X^3_{sub} is the state vector of waist-mounted modules. The overall state vector of each subsystem contains state values with dimension of 16:

$$\delta X^i_{sub} = \begin{bmatrix} (\delta p^n)_{1\times3} & (\delta v^n)_{1\times3} & \boldsymbol{\phi}_{1\times3} & (\varepsilon^b_g)_{1\times3} & (\nabla^b_a)_{1\times3} & b_h \end{bmatrix}^T \tag{28}$$

where δp^n, δv^n and $\boldsymbol{\phi}$ represent the state error of 3D position, walking velocity, and attitude, respectively; ε_g, $_a$, and b_h represent related biases of the gyroscope, accelerometer, and barometer, respectively.

The low-cost sensor-based INS mechanization is subjected to cumulative and divergence errors, making it unsuitable for standalone applications. In the proposed DMDD structure, an unscented Kalman filter (UKF) is ultimately employed in the data integration process. Multi-level observations and constraints, which can depict the overall motion characteristics and relationships between different sensors and ultrasonic modules, are extracted and modeled as the observation equation:

1) The spatial–temporal (ST) model predicted motion-related walking speed reference is utilized as the first-level observation:

$$\begin{cases} \delta Z^n_v = v^n_{ST} - v^n_{INS} \\ \delta Z^n_p = p^n_{ST} - p^n_{INS} \end{cases} \tag{29}$$

where v^n_{ST} and p^n_{ST} represent the ST model output speed and location information, respectively, v^n_{INS} and p^n_{INS} are the INS originated walking speed and location information, respectively.

2) To lessen the effects of the influenced magnetic field, this paper utilizes the magnetic observation vector of the WPS module from the identified quasi-static magnetic field (QSMF) to calibrate the heading error (Sun et al. 2021):

$$\delta \boldsymbol{Z}^n_m = \boldsymbol{C}^b_{n,k} \cdot \boldsymbol{m}^b_k - \boldsymbol{C}^b_{n,1} \cdot \boldsymbol{m}^b_{k,1} \tag{30}$$

where $\boldsymbol{C}^b_{n,1}$, $\boldsymbol{C}^b_{n,k}$, m^b_k, and $m^b_{k,1}$ represent the attitude matrix and magnetic field vector extracted from the first epoch of QSMF periods and other epochs, respectively.

3) In this paper, a height-related zero-velocity update method (H-ZUPT) is presented to eradicate the altitude estimation drift, in which the bias of the barometer is modeled as a random walk procedure, and the state update equation is formulated as (Qi et al. 2022):

$$\begin{bmatrix} \dot{h} \\ \dot{b}_h \end{bmatrix} = \begin{bmatrix} w_h \\ -\frac{1}{\tau_{b_h}} b_h + v_{b_h} \end{bmatrix} \tag{31}$$

where w_h is the noise of acquired altitude; τ_{b_h} and v_{b_h} are the correlation time and the driving noise of the random walk process, respectively. When the height-related QS periods are detected, the observation equation of H-ZUPT is modeled as:

$$\overset{b}{h} - \hat{h}_0 = \delta h + b_h + n_{h_b} \tag{32}$$

where $\overset{b}{h}$ indicates the barometer originated altitude; $\hat{h}_0$ indicates the first epoch of height-related QS phases.

4) Considering that the SL constraint is used to restrict the drift error when the pedestrian walks straight forward, and the heading observations calculated by adjacent step phases provided by S-MPS subsystems are further integrated into the final DMDD for enhanced straightline recognition:

$$L_\theta = \begin{cases} 1, \max\left\{\theta^w - mean(\theta^f)\right\} < T_\theta \\ 0, others \end{cases} \tag{33}$$

where θ^w and θ^f indicate the reference heading provided by waist-mounted and foot-mounted modules, respectively.

5) In this research, taking into account the relationship between different sensors and ultrasonic modules, the hybrid maximum and minimum ranging distance observations provided by various S-MPSs, and ultrasonic ranging are modeled as constraints to improve positioning accuracy. Assuming that the sensor module originated distances R_1 and R_2 represent the distances between different sensor modules, and D_{ultra} represents the ultrasonic ranging, the minimum distance among the three modules is modeled as:

$$\delta Z_{\min} = R_1 + R_2 - D_{ultra} \tag{34}$$

In typical walking scenarios, the calculated distances provided by ultrasonic ranging and sensor modules are equal.

For outlier instances in ultrasonic ranging, the non-light-of-sight (NLOS) effect is incorporated into the

distance observations based on ultrasonic ranging. Hence, for the maximum distance, the ranging result among foot-mounted modules is utilized as the reference distance value, amalgamated with a control factor to offset the initial bias between step length and calculated distance:

$$\delta Z_{\max} = R_1 + R_2 - D_{FPS} + \delta_0 \tag{35}$$

To sum up, in the ultimate DMDD-amplified MP-TMDS, to integrate all the movement attributes offered by various nodes and take into account the limiting connection between different sensor nodes, the subsequent actions are implemented. Initially, INS mechanization is utilized as the core location–attitude update algorithm, with the error measurements of three different sensor modules modeled as the overall state vector of MP-TMDS. Subsequently, to effectively decrease the cumulative error of the overall system, observations and constraints derived from distributed sensor modules and pedestrian movement data are employed, aiming at comprehensive pedestrian movement constraint features. These encompass the ST network predicted movement modes and walking velocity, QSMF, H-ZUPT, enhanced SL, and minimum and maximum distance observations.

4. Experimental results

In this section, extensive experiments are carried out to validate the accuracy of the presented S-NPS, D-NPS, and the comprehensive MP-TMDS. Three distinct seamless scenarios are selected as the real-world test sites, and comparative tests are conducted alongside SOTA methods and frameworks. In the experiments, distributed sensor modules are placed on different feet and waist parts of the human body, as depicted in Figure 4 (Qi et al. 2024), and all the sensor and ultrasonic data acquired from dual foot-mounted modules are sent to the waist-mounted module using wired transmission method for time synchronization. The precision specifications of the MEMS sensors incorporated within the S-NPS are detailed in Table 1.

Figure 4. Hardware deployment of MP-TMDS.

4.1. Accuracy evaluation of S-MPS

In this paper, multi-level constrains and observations are applied to decrease the drift error inherent in the INS mechanization utilized within the S-NPS. To assess the efficacy of this approach, an archetypal indoor environment, comprising a hallway and office space, is selected as the testing ground. Additionally, a publicly available dataset, collected within a three-dimensional office building, is used to compare the performance of various algorithms under identical conditions. The pedestrian traversed the designated offices and hallways for a period of 15 min (Website: http://www.i2nav.com/index/newListDetail_zw.do?newskind_id=13a8654e060c40c69e5f3d4c13069078&newinfo_id=c54efa006a33426d991235801b427f6d). The inertial module used in the experiment and the different test scenarios are depicted in Figure 5. The calibrated biases for the gyroscope and accelerometer are illustrated in Figure 6. The final positioning precision and the associated errors among varying levels of constraints are juxtaposed in Figure 7(a,b).

Figure 7 indicates the performance comparison results of trajectory and related error. As illustrated in Figure 7(a), the suggested multi-level constraints notably improve the positioning precision by adjusting the divergence error of inertial sensors,

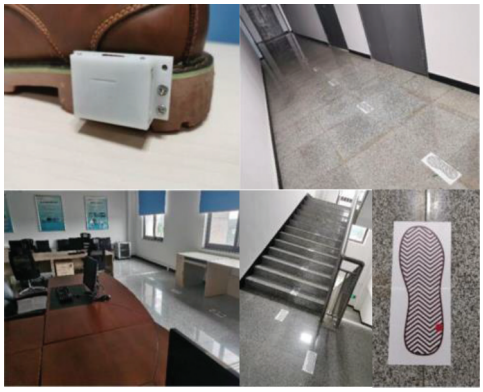

Figure 5. Experimental environments of public dataset (Niu et al. 2019).

Table 1. Precision specifications of different sensors.

Specification	Gyroscope	Accelerometer	Barometer	Ultrasonic
Sampling rate	200 Hz	200 Hz	10 Hz	100 Hz
Dynamic range	2000°/s	16 g	300–1100 hPa	3–500 mm
Bias instability	10°/h	0.03 mg	–	–
White noise	$0.16^\circ/\sqrt{h}$	$0.02m/s/\sqrt{h}$	–	–

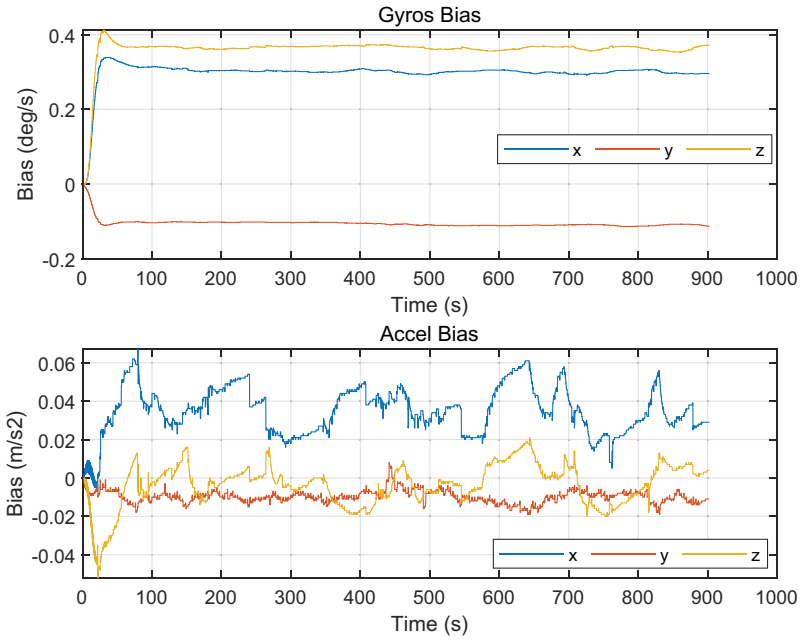

Figure 6. Calibrated biases of gyroscope and accelerometer.

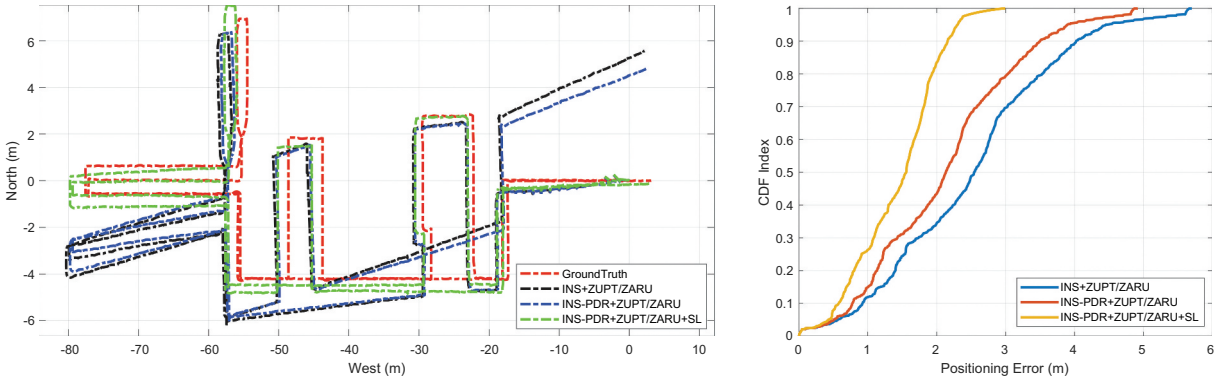

(a) Positioning trajectory comparison (b) Positioning error comparison

Figure 7. Positioning trajectory and error comparison.

surpassing the other two constraints. Figure 7(b) contrasts the localization error under different constraints. The ultimate assessed localization error of the presented multi-level constraint model is less than 1.85 m in 75% of instances, which is significantly less than the INS-PDR+ZUPT/ZARU model (2.78 m under 75%) and the original INS +ZUPT/ZARU model (3.27 m under 75%).

4.2. Accuracy evaluation of D-MPS

This paper presents the bidirectional long short-term memory (Bi-LSTM) network as a strategy to mitigate the impact of ultrasonic ranging outliers, which may arise from hardware malfunctions or non-line-of-sight (NLOS) effects encountered during pedestrian movement. The refined ultrasonic data are subsequently integrated with dual-sensor nodes to enhance positioning accuracy. In this work, the dimension of the input vector of Bi-LSTM is set as 7, the length of each round of input is set as 200 under 1 s time window, the step-length of model training is set as 0.03, and the hidden size is set as 100. The efficiency of the Bi-LSTM-based anomaly detection mechanism is illustrated in Figure 8.

In this case, 10 distinct sets of paths are carried out to assess the detection precision of the suggested detector, with the conventional threshold-based

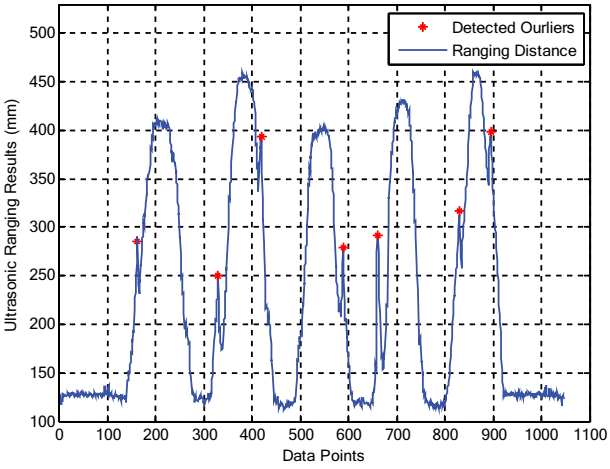

Figure 8. Bi-LSTM based ultrasonic outlier detection.

Table 2. Detection ratio of ultrasonic outlier detectors.

Route	Bi-LSTM	Threshold
T01	89.2%	86.3%
T02	91.5%	89.2%
T03	92.1%	89.6%
T04	90.5%	88.1%
T05	88.7%	87.2%
T06	89.8%	86.5%
T07	91.3%	90.2%
T08	90.7%	89.9%
T09	88.2%	85.7%
T10	91.4%	86.8%
Average	90.34%	87.95%

anomaly detector used for comparison (Qi et al. 2023). A thorough accuracy comparison under various walking paths and algorithms is displayed in Table 2.

Table 2 shows that the suggested Bi-LSTM-based ultrasonic anomaly detector attains a higher anomaly detection precision compared to the threshold-based method, with an average accuracy of 90.34% across 10 different test walking paths.

To compare the performance of the presented S-NPS, DFM-NU, and DFM-U, we carry out a long-term experiment to evaluate the effectiveness of the dual-node-based integration model. The walking path of the tests is portrayed in Figure 9. The walking path starts at point A, goes through points B, C, D, E, F, and returns to point A. This entire path is repeated 10 times for long-term performance assessment, and the estimated paths and accuracies provided by combinations of different sensor nodes are displayed in Figure 10.

Figure 10 describes the comparison of positioning trajectories and related errors. As seen from Figure 10 (b), the proposed dual sensor node-based positioning model notably improves the effectiveness of the S-MPS, mainly by eradicating the systematic heading drift caused by a single node. Moreover, the integration of ultrasonic distance measurements further enhances the accuracy of D-MPS. The positioning accuracies of the three different models achieve 2.11 m, 3.81 m, and 5.68 m at the 75% percentile, respectively.

4.3. Accuracy evaluation of MP-TMDS

This paper presents the hybrid spatial–temporal network to estimate human movement modes and related walking velocity based on a combination of distributed sensors and ultrasonic modules. To estimate the effectiveness of the proposed spatial–temporal network, the temporal network LSTM (Liu et al. 2022), and a typical spatial graph (SG) network (Chen et al. 2021b) is employed as baseline models. The hybrid velocity and motion dataset is generated based on the reference of high-precision Lidar device and SLAM algorithm, with manually annotated motion patterns (Bao et al. 2022). In the proposed hybrid spatial–temporal network, the dimension of the input vector of Bi-LSTM is set as 13 including dual IMU and ultrasonic values, the length of each round of input is set as 200 under 1 s time window, the step-length of model training is set as

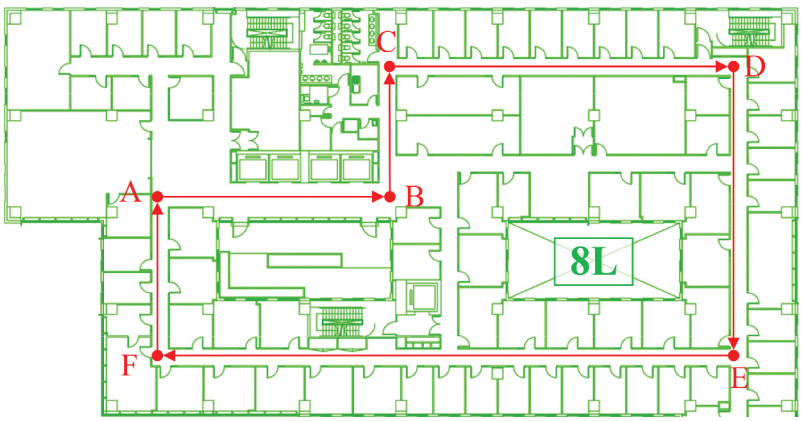

Figure 9. Test route of sensor node.

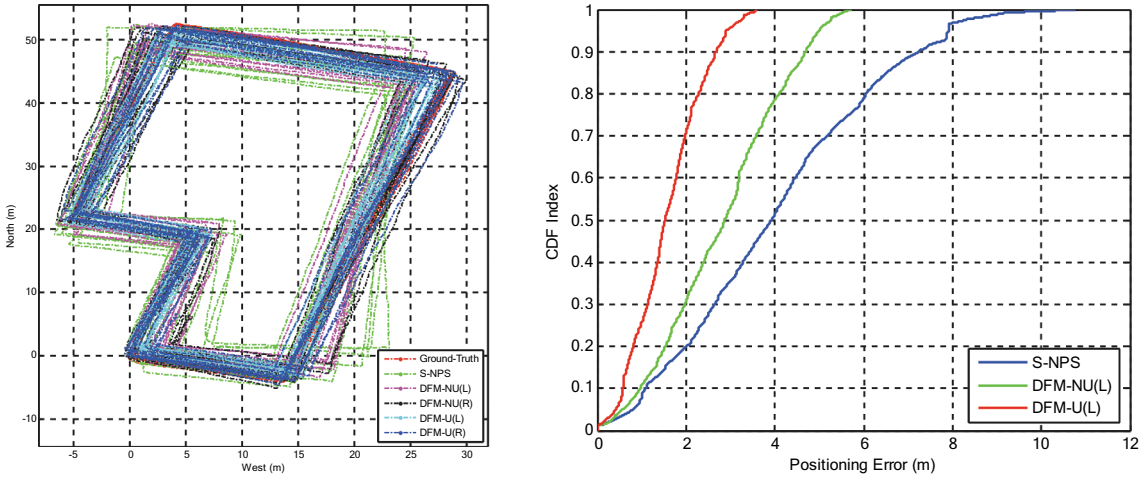

(a) Positioning trajectories (b) Positioning errors

Figure 10. Trajectory and error comparison.

Table 3. Accuracy of motion mode detection.

Motion/Model	ST	LSTM	SG
Static	100%	100%	100%
Typical walking	100%	100%	100%
Running	100%	100%	100%
Backward walking	92.8%	89.6%	88.7%
Lateral walking	91.5%	87.2%	86.8%
Go up stairs	98.7%	95.8%	94.9%
Go down stairs	99.1%	96.3%	93.6%
Taking elevator	98.4%	97.8%	97.5%
Average	97.6%	95.8%	95.2%

Table 4. Walking velocity prediction error comparison.

Index/Model	ST	LSTM	SN
Mean (m/s)	0.032	0.043	0.047
Std (m/s)	0.021	0.024	0.026
Max (m/s)	0.085	0.113	0.124
Min (m/s)	0.003	0.009	0.012
75th (m/s)	0.048	0.061	0.068
Median (m/s)	0.025	0.031	0.036

0.03, and the hidden size of LSTM and GCN is set as 100 and 50, respectively. The comparison results of predicted success rate of human movement modes and walking velocity with baseline models are described in Table 3 and Table 4, respectively:

Table 2 and Table 3 show that the suggested spatial–temporal model attains the highest precision in movement mode detection and walking pace prediction compared to two existing models, including the temporal model LSTM and a typical spatial graph model. The calculated walking speed prediction error is less than 0.048 in 75%, and the average precision of human movement detection reaches 97.6%.

Finally, the proposed MP-TMDS is assessed under complex real-world test scenarios and contrasted with SOTA D-MPS methods. The evaluation path contains multi-floor indoor scenarios as depicted in Figures 9 and 11. Testers start at point A, walk pass points B–A, H–G, and back to point A. The time period and total route length are 380 s and 500 m.

The effectiveness of the suggested MP-TMDS in predicting paths under different sensor nodes, including modules mounted on the waist and foot, is portrayed in Figure 12(a,b)

Figure 12 indicates that the proposed MP-TMDS structure exhibits enhanced performance compared to

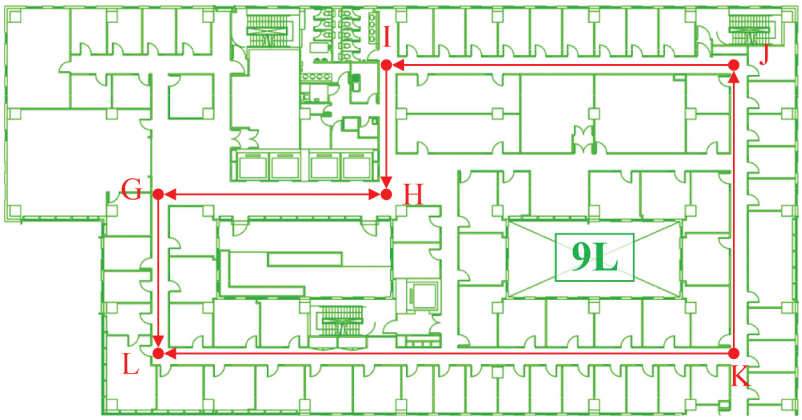

Figure 11. Test path in 9th floor.

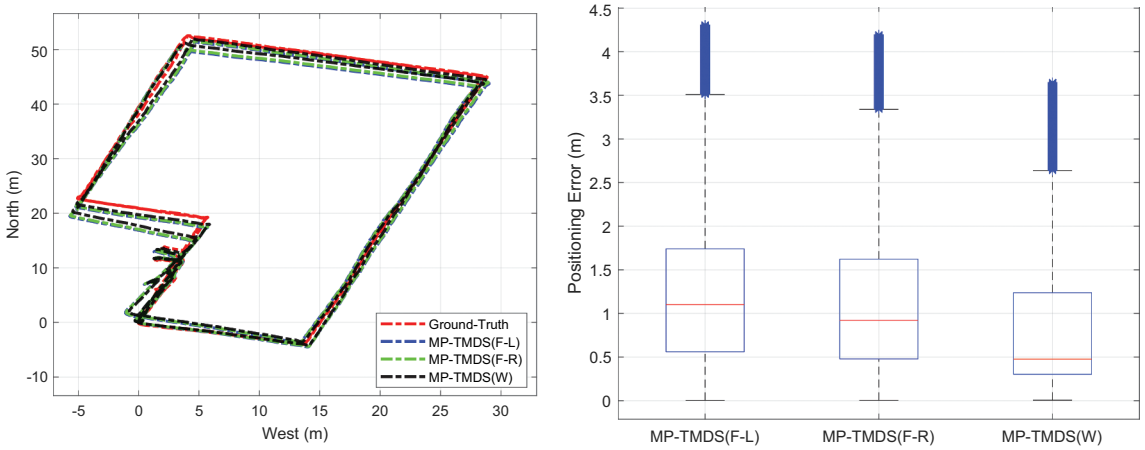

(a) Positioning trajectories of MP-TMDS (b) Positioning errors of MP-TMDS

Figure 12. Positioning trajectories and errors of MP-TMDS.

the single-sensor module and dual-sensor nodes, with the integrated positioning error effectively diminished through the application of multi-level constraints and observations. The final estimated positioning accuracies of the presented MP-TMDS structure under foot-mounted and waist-mounted modules achieve 1.74 m, 1.62 m, and 1.24 m at the 75% level.

Finally, the overall MP-TMDS is compared with SOTA D-NPS algorithms: f^2 IMU-R (M. Zhu, Wu, and Luo 2021), FPS-DU (Qi et al. 2023), and H-PPS (Qi et al. 2024), under the same test path, with the evaluated localization errors provided by different D-NPS algorithms as:

Figure 13 shows that the developed MP-TMDS displays superior tracking effectiveness compared to existing D-NPS methods. The evaluated localization errors in the tested scenarios achieve 1.24 m in 75% (MP-TMDS), 1.52 m in 75% (H-PPS), 1.75 m in 75% (f^2 IMU-R), and 1.87 m in 75% (FPS-DU), which improve the final positioning accuracy by more than 18.4% compared with state-of-the-art algorithms.

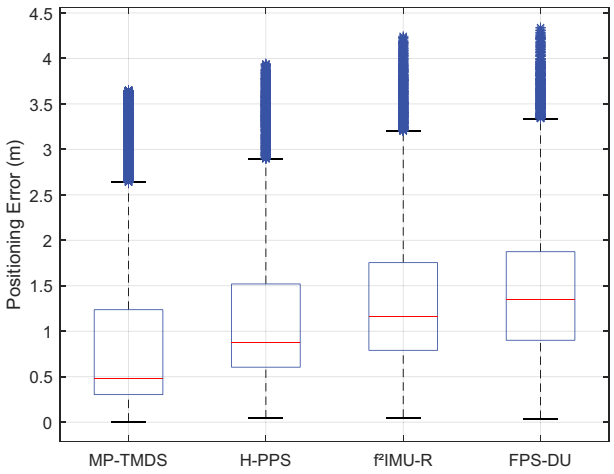

Figure 13. Positioning errors of existing algorithms.

For the sensitivity of proposed MP-TMDS structure, the performance of MP-TMDS is affected following factors: the first is the complexity of positioning environments, the harsh environment that contains complex layout and magnetic interference will decrease the accuracy of multi-node positioning; the second of the distribution of IMU nodes, since the combination of dual feet-mounted nodes and waist-mounted node show the high accuracy, the other distribution of IMU nodes such as head and thigh will also be potentially feasible; the third is the noise level of selected inertial sensors, which will lead to the changes in positioning base accuracy due to the level of the inertial sensors; the last is the robustness of motion detection, which is affected by the more complex human motion modes, and leads to the decreased accuracy of walking speed estimation.

In summary, this paper proposes the MP-TMDS structure that combines the distributed inertial sensor nodes together and improves the positioning accuracy of the overall system compared with a single inertial-sensor node. Specially, the physical model is proposed that supports both foot-mounted modules and waist-mounted modules, using the accurate heading information provided by waist-mounted modules and walking speed information provided by foot-mounted modules to overcome the disadvantages of each. A spatial–temporal network is proposed to extract the motion features of the overall human body from distributed inertial sensor nodes and combined with a physical model to enhance the accuracy and robustness of the overall MP-TMDS.

Disclosure statement

No potential conflict of interest was reported by the author(s).

Funding

This work is supported by the National Natural Science Foundation of China [Grant number 52175531], The Hong Kong Polytechnic University [Grant number P0045937]; Open Fund of State Key Laboratory of Information Engineering in Surveying, Mapping and Remote Sensing, Wuhan University [Grant number 23P03], and in part by the Science and Technology Research Program of Chongqing Municipal Education Commission [Grant numbers KJQN202000605 and KJZD-M202000602].

Notes on contributors

Lin Qi received the M.S. degree and the Ph.D. degree from the Chongqing University and Chongqing University of Posts and Telecommunications, respectively. She is currently a Senior Engineer in the Department of Solid-State Image Sensors at the 44th Research Institute of China Electronics Technology Group Corporation in Chongqing, China. Her research interests include inertial positioning and navigation technology, signal processing, and fusion technology and has published over 10 SCI-indexed journals and conference articles.

Yi Zhang received a Ph.D. degree from The Hong Kong Polytechnic University. She is currently a Postdoctoral Fellow in the Department of Building and Real Estate, The Hong Kong Polytechnic University. Her research focuses on knowledge management, big data cooperative assets, and corporate digital transformation. She has published over 10 SCI/SSCI-indexed journal articles. Holding professional certifications as a Certified Public Accountant (CPA) and HKICPA member, she possesses extensive practical experience in financial and risk management. Her industry engagements include participating in electronic financial system development for Fortune 500 enterprises, bankruptcy liquidation assessment, and tax risk control projects for financial institutions.

Yu Liu received the M.S. and Ph.D. degrees from the Chongqing University. He is currently a Professor at the Chongqing University of Posts and Telecommunication. His research interests include inertial sensors, navigation systems, and signal processing. He has received more than 20 national and provincial/ministerial-level science and technology awards (including 6 at the national level), published 4 monographs and books, applied for over 30 national invention patents with 14 granted, and published more than 70 high-level papers as the first author (over 50 of which are indexed by SCI, EI, and other databases).

Izzy Yi Jian is currently is an Assistant Professor in the Department of Social Sciences and Policy Studies at the Education University of Hong Kong and the Vice President & Director of Happy Ageing Lab Foundation. She came from Architecture background and earned her Ph.D. from the Department of Building and Real Estate, and Research Institute of Sustainable Urban Development (RISUD), Hong Kong Polytechnic University. She is also an Ernst Mach Global Research Fellow at the Department of Geography and Regional Research, the University of Vienna, in 2021. Her research and teaching interests include spatial justice, inclusive design, and media geography.

Yue Yu is currently a research Assistant Professor in the Department of Land Surveying and Geo-Informatics. He received the B.S. and M.S. degrees from the Chongqing University of Posts and Telecommunications and received dual Ph.D. degrees from both Wuhan University and the Hong Kong Polytechnic University. He has published more than 70 papers in SCI journals and conference papers. His research interests include inertial positioning and navigation technology, indoor positioning and navigation technology based on chance signal, signal processing, and fusion technology.

Liang Chen is currently a Professor at the State Key Laboratory of Surveying, Mapping and Remote Sensing Information Engineering, Wuhan University. He was a Senior Researcher at the Finnish Geodesy Institute, Deputy Head of the Sensors and Indoor Navigation Research Group, and Research Leader at the Finnish Laser Radar National Excellent Innovation Center. His research interests include navigation based on new signal theory and methods, smartphone ubiquitous positioning and indoor and outdoor seamless localization and navigation.

Ruizhi Chen is currently a Professor at the School of Data Science, The Chinese University of Hong Kong (Shenzhen). He is a member of the Finnish Academy of Science and Letters. He is one of the World's Top 2% Scientists by Sandford. He was the Director of the State Key Laboratory of Information Engineering in Surveying, Mapping and Remote Sensing at Wuhan University, China, an Endowed Chair Professor at Texas A&M University Corpus Christ, US, and the Head & Professor of the Department of Navigation and Positioning at the Finnish Geodetic Institute, Finland. Dr. Chen's research interests include indoor positioning and location-based services. He has published two books and 200+ SCI papers. His research results were selected as cover stories two times in "GPS World" in US.

References

Bao, S., W. Shi, P. Chen, H. Xiang, and Y. Yu. 2022. "A Systematic Mapping Framework for Backpack Mobile Mapping System in Common Monotonous Environments." *Measurement* 197:111243. https://doi.org/10.1016/j.measurement.2022.111243.

Barbieri, L., M. Brambilla, A. Trabattoni, S. Mervic, and M. Nicoli. 2021. "UWB Localization in a Smart Factory: Augmentation Methods and Experimental Assessment"." *IEEE Transactions on Instrumentation and Measurement* 70:1–18. https://doi.org/10.1109/TIM.2021.3074403.

Chen, C., Z. Zhu, and A. Hammad. 2020. "Automated Excavators Activity Recognition and Productivity Analysis from Construction Site Surveillance Videos." *Automation in Construction* 110:103045. https://doi.org/10.1016/j.autcon.2019.103045.

Chen, L., X. Zhou, F. Chen, L. L. Yang, and R. Chen. 2021a. "Carrier Phase Ranging for Indoor Positioning with 5G NR Signals." *IEEE Internet of Things Journal* 9 (13): 10908–10919. https://doi.org/10.1109/JIOT.2021.3125373.

Chen, Y. L., I. J. Yang, L. C. Fu, J. S. Lai, H. W. Liang, and L. Lu. 2021b. "IMU-Based Estimation of Lower Limb Motion Trajectory with Graph Convolution Network." *IEEE Sensors Journal* 21 (21): 24549–24557. https://doi.org/10.1109/JSEN.2021.3115105.

Kuang, J., T. Li, Q. Chen, B. Zhou, and X. Niu. 2022. "Consumer-Grade Inertial Measurement Units Enhanced Indoor Magnetic Field Matching Positioning Scheme." *IEEE Transactions on Instrumentation and*

Measurement 72:1–14. https://doi.org/10.1109/TIM.2022.3221754.

Liu, Z., R. Chen, C. Jiang, F. Ye, G. Guo, L. Chen, and X. Lin. 2024. "Submeter-Level TOF-Based Acoustic Positioning of Moving Objects with Chirp-Based Doppler Shift Compensation." *IEEE Internet of Things Journal* 11 (12): 21916–21929. https://doi.org/10.1109/JIOT.2024.3377435.

Liu, Z., W. Shi, Y. Yu, P. Chen, and B. Y. Chen. 2022. "A LSTM-Based Approach for Modelling the Movement Uncertainty of Indoor Trajectories with Mobile Sensing Data." *International Journal of Applied Earth Observation and Geoinformation* 108:102758. https://doi.org/10.1016/j.jag.2022.102758.

Mehrabian, H., and R. Ravanmehr. 2023. "Sensor Fusion for Indoor Positioning System Through Improved RSSI and PDR Methods." *Future Generation Computer Systems* 138:254–269. https://doi.org/10.1016/j.future.2022.09.003.

Niu, X., Y. Li, J. Kuang, and P. Zhang. 2019. "Data Fusion of Dual Foot-Mounted IMU for Pedestrian Navigation." *IEEE Sensors Journal* 19 (12): 4577–4584. https://doi.org/10.1109/JSEN.2019.2902422.

Niu, X., T. Liu, J. Kuang, Q. Zhang, and C. Guo. 2021. "Pedestrian Trajectory Estimation Based on Foot-Mounted Inertial Navigation System for Multistory Buildings in Postprocessing Mode." *IEEE Internet of Things Journal* 9 (9): 6879–6892. https://doi.org/10.1109/JIOT.2021.3113398.

Pham, T. T., and Y. S. Suh. 2021. "Walking Step Length Estimation Using Waist-Mounted Inertial Sensors with Known Total Walking Distance." *IEEE Access* 9:85476–85487. https://doi.org/10.1109/ACCESS.2021.3087721.

Qi, L., Y. Liu, C. Gao, T. Feng, and Y. Yu. 2024. "Hybrid Pedestrian Positioning System Using Wearable Inertial Sensors and Ultrasonic Ranging." *Defence Technology* 33:327–338. https://doi.org/10.1016/j.dt.2023.11.006.

Qi, L., Y. Yu, Y. Liu, C. Gao, and T. Feng. 2022. "Precise 3D Foot-Mounted Indoor Localization System Using Commercial Sensors and Map Matching Approach." *Measurement Science and Technology* 33 (11): 115117. https://doi.org/10.1088/1361-6501/ac87c5.

Qi, L., Y. Yu, Y. Liu, C. Gao, T. Feng, J. Hui, and S. Wang. 2023. "A Robust Foot-Mounted Positioning System Based on Dual IMU Data and Ultrasonic Ranging." *IEEE Sensors Journal* 23 (4): 4085–4095. https://doi.org/10.1109/JSEN.2022.3232613.

Qian, K., Z. Zhang, Y. Yamamoto, and B. W. Schuller. 2021. "Artificial Intelligence Internet of Things for the Elderly: From Assisted Living to Health-Care Monitoring." *IEEE Signal Processing Magazine* 38 (4): 78–88. https://doi.org/10.1109/MSP.2021.3057298.

Qin, T., P. Li, and S. Shen. 2018. "VINS-MONO: A Robust and Versatile Monocular Visual-Inertial State Estimator." *IEEE Transactions on Robotics* 34 (4): 1004–1020. https://doi.org/10.1109/TRO.2018.2853729.

Qiu, S., H. Zhao, N. Jiang, D. Wu, G. Song, H. Zhao, and Z. Wang. 2022. "Sensor Network Oriented Human Motion Capture via Wearable Intelligent System." *International Journal of Intelligent Systems* 37 (2): 1646–1673. https://doi.org/10.1002/int.22689.

Shi, W., Y. Yu, Z. Liu, R. Chen, and L. Chen. 2022. "A Deep-Learning Approach for Modelling Pedestrian Movement Uncertainty in Large-Scale Indoor Areas." *International Journal of Applied Earth Observation and Geoinformation* 114:103065. https://doi.org/10.1016/j.jag.2022.103065.

Sun, X., H. Ai, J. Tao, T. Hu, and Y. Cheng. 2021. "BERT-Adloc: A Secure Crowdsourced Indoor Localization System Based on BLE Fingerprints." *Applied Soft Computing* 104:107237. https://doi.org/10.1016/j.asoc.2021.107237.

Wu, Y., J. Kuang, and X. Niu. 2022. "Wheel-Ins2: Multiple MEMS IMU-Based Dead Reckoning System with Different Configurations for Wheeled Robots." *IEEE Transactions on Intelligent Transportation Systems* 24 (3): 3064–3077. https://doi.org/10.1109/TITS.2022.3220508.

Yu, N., Y. Li, X. Ma, Y. Wu, and R. Feng. 2019. "Comparison of Pedestrian Tracking Methods Based on Foot-and Waist-Mounted Inertial Sensors and Handheld Smartphones." *IEEE Sensors Journal* 19 (18): 8160–8173. https://doi.org/10.1109/JSEN.2019.2919721.

Yu, Y., W. Shi, R. Chen, L. Chen, S. Bao, and P. Chen. 2022. "Map-Assisted Seamless Localization Using Crowdsourced Trajectories Data and Bi-LSTM Based Quality Control Criteria." *IEEE Sensors Journal* 22 (16): 16481–16491. https://doi.org/10.1109/JSEN.2022.3190387.

Yu, Y., Y. Zhang, L. Chen, and R. Chen. 2023. "Intelligent Fusion Structure for Wi-Fi/BLE/QR/MEMS Sensor-Based Indoor Localization." *Remote Sensing* 15 (5): 1202. https://doi.org/10.3390/rs15051202.

Zhang, P., Y. Li, Y. Zhuang, J. Kuang, X. Niu, and R. Chen. 2023. "Multi-Level Information Fusion with Motion Constraints: Key to Achieve High-Precision Gait Analysis Using Low-Cost Inertial Sensors." *Information Fusion* 89:603–618. https://doi.org/10.1016/j.inffus.2022.09.009.

Zhu, M., Y. Wu, and S. Luo. 2021. "F²IMU-R: Pedestrian Navigation by Low-Cost Foot-Mounted Dual IMUs and Interfoot Ranging." *IEEE Transactions on Control Systems Technology* 30 (1): 247–260. https://doi.org/10.1109/TCST.2021.3063533.

Zhu, R., J. Lin, B. Becerik-Gerber, and N. Li. 2020. "Human-Building-Emergency Interactions and Their Impact on Emergency Response Performance: A Review of the State of the Art." *Safety Science* 127:104691. https://doi.org/10.1016/j.ssci.2020.104691.